ADVANCED MATERIALS
www.advmat.de

Plasmonic Metaparticles on a Blackbody Create Vivid Reflective Colors for Naked-Eye Environmental and Clinical Biodetection

Mady Elbahri, Moheb Abdelaziz, Shahin Homaeigohar, Abdou Elsharawy, Mehdi Keshavarz Hedayati, Christian Röder, Mamdouh El Haj Assad, and Ramzy Abdelaziz*

Plasmonic dipoles are famous for their strong absorptivity rather than their reflectivity. Here, the as-yet unknown specular reflection and the Brewster effect of ultrafine plasmonic dipoles, metaparticles, are introduced and exploited as the basis of new design rules for advanced applications. A configuration of "Plasmonic metaparticles on a blackbody" is demonstrated and utilized for the design of a tailored perfect-colored absorber and for visual detection of environmental dielectrics that is not readily done by extinction plasmonics. Moreover, the Plasmonic Brewster Wavelength (PBW) effect is introduced as a new platform for the naked-eye and bulk biodetection of analytes. The technique operates based on slight changes of molecular polarizability which is not detectable via conventional plasmon resonance techniques. As a specific highlight, the clinical applicability of the PBW method is demonstrated while addressing the transduction plasmonic techniques' challenge in detection of bulk refractive index changes of the healthy and diseased human serum exosomes. Finally, the sputtering-based fabrication method used here is simple, inexpensive, and scalable, and does not require the sophisticated patterning approach of lithography or precise alignment of light coupling for the biodetection.

The specular reflection color in nature is a peculiar interference optical phenomenon originated from several optical processes including reflection grating, diffraction grating, coherent light scattering by periodic structures, etc.[1] In contrast to such complex processes, creation of the specular reflection colors by amorphous plasmonic dipoles can be an efficient while simple alternative. Although tiny plasmonic dipoles with sizes below 10 nm are well known for their strong absorption potential,[2–4] they have never been considered for creation of the vivid interference plasmonic colors. In this regard, some involved fundamental aspects are still unexplored that could be employed for creation of a diverse range of new properties. For example, the plasmonic specular reflection and the plasmonic Brewster phenomenon occurring at the resonance frequency are interesting new

Prof. M. Elbahri, M. Abdelaziz, Dr. S. Homaeigohar, Dr. R. Abdelaziz
Nanochemistry and Nanoengineering
School of Chemical Engineering
Department of Chemistry and Materials Science
Aalto University
Kemistintie 1, 00076 Aalto, Finland
E-mail: mady.elbahri@aalto.fi
Prof. M. Elbahri, M. Abdelaziz, Dr. M. K. Hedayati
Nanochemistry and Nanoengineering Group
Institute for Materials Science
Faculty of Engineering
University of Kiel
Kaiserstrasse 2, 24143 Kiel, Germany
Prof. M. Elbahri
Zewail City of Science and Technology
Sheikh Zayed District, 12588 Giza, Egypt
Dr. A. Elsharawy
Institute of Clinical Molecular Biology
University of Kiel
24105 Kiel, Germany
Dr. C. Röder
Institute for Experimental Cancer Research
University of Kiel
24105 Kiel, Germany
Dr. A. Elsharawy
Faculty of Sciences
Division of Biochemistry
Chemistry Department
Damietta University
34511 New Damietta City, Egypt
Dr. M. K. Hedayati
Department of Micro- and Nanotechnology
Technical University of Denmark
Kongens Lyngby DK-2800, Denmark
Prof. M. E. H. Assad
SREE Department
University of Sharjah
27272 Sharjah, United Arab Emirates
Dr. R. Abdelaziz
Department of Ceramics and Building Materials
National Research Center (NRC)
Dokki 12622, Cairo, Egypt

DOI: 10.1002/adma.201704442

features. These versatile properties can bloom the design rules in the progressive fields of plasmonics. In this context, they can lead to generation of new, efficient perfect solar absorbers[5–9] in diverse colors, for instance. Also, they can be employed for induction of glowing interference plasmonic colors, with no need to use sophisticated fabrication and patterning methods.[10–14] Such a feasibility can be beneficial to overcome the important shortcoming of the recently developed plasmonic biosensors.[15–19] The plasmonic biosensors introduced in the literature are able to detect analytes solely at a molecular level (e.g., surface detection via antibody/antigen functionalization) and within an enhanced local field of only a few nanometers.[15–20] Bulk detection of biosamples based on plasmonic materials, which is essential for commercialization of the technique and its clinical implementation, has been rarely considered. The reason is that the localized plasmonic detection is not feasible based on bulk refractive index (RI) variations and with a minor change of molecular polarizability. This situation applies even when the sophisticated technique of the surface plasmon polariton in an ATR Kretschmann configuration (whose wavelength shift is ≈0.5–1 nm) is exploited.[21]

Here, we aim to manifest that ultrafine plasmonic (artificial) dipoles, i.e., pure absorbers, act as macroscopic antennas and behave as quasimetallic nanomirrors. Accordingly, they create a specular reflection plasmonic color at the resonance frequency even if they are randomly distributed on a blackbody. Similar to the extinction-based plasmonic response, the properties can be tailored by type and filling factor of the plasmonic nanoparticles and the host medium's polarity. To prove our hypothesis concerning emergence of the plasmonic color solely from the plasmonic nanoparticles, several systems based on silver (Ag) nanoparticles embedded dielectric host, and Ag- and gold (Au)-free nanoparticles on a substrate were studied. Thus, in fact, the role of the interface on appearance of the specularly radiated colors was elaborated. Ag and Au are the most widely used plasmonic materials and can be selectively employed in various targeted applications. In this study, Ag was implemented for the design of a perfect-colored absorber with the emissivity comparable to a blackbody's in the mid-IR. Whereas, the most chemically stable Au nanoparticles were chosen for a biosensing purpose. Indeed, the specular reflection gives rise to the plasmonic Brewster effect that can be exploited in the design of a platform for environmental/bio detection of analytes in bulk states not attainable by the extinction mode of the localized plasmon. The effect enables a surface inspection function by light reflection. Additionally, volume detection is realized via the Brewster effect and by irradiation of p-polarized light. Hence, visual detection of environmental and biological analytes (e.g., the serum exosomes associated with diseases) comes into practice.

The specular reflection of ultrafine dipoles is realized by the microscopic interference of the radiated Hertzian dipoles[22–24] caused by fluctuations of charges and current.[25] As a consequence of the interference, the material becomes an anisotropic-polarized medium able to store energy while radiating the electromagnetic waves (i.e., the "real part" of RI) caused by the propagation delay. The collective oscillation of the dipoles leads to cooperative dipolar coupling. Such coupling results in a resonating specular reflection, even if the dipoles are randomly distributed or the substrate is a blackbody (**Figure 1**a). Figure 1b,c illustrates a single Hertzian dipole oscillator and coherent coupling of six disordered

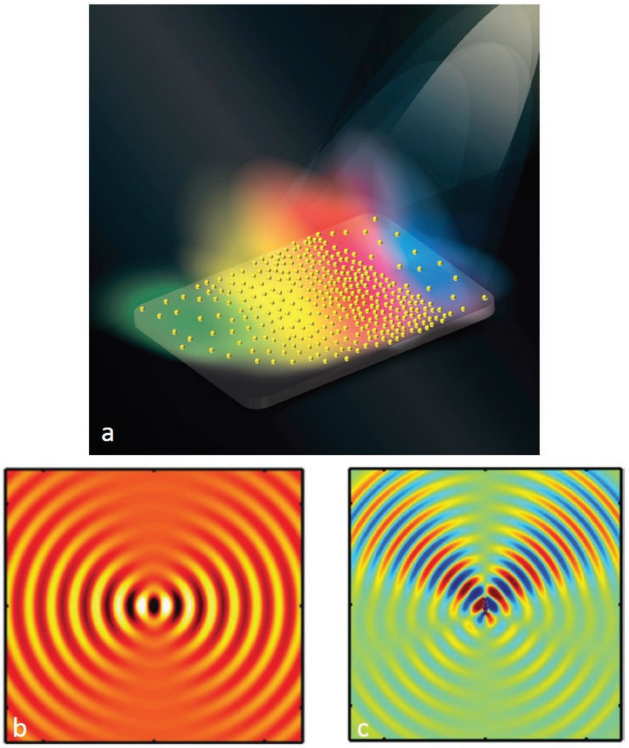

Figure 1. The specular reflection color generation mechanism. a) Schematic demonstration of tailored specular colors radiated from the plasmonic nanoparticles with different filling factors deposited on a blackbody. b) The Hertzian electric dipole antennas localize the electrical current and thus radiate an electric field. c) The interference and directed light radiation of six closely spaced Hertzian dipoles.

Hertzian dipoles in close proximity, respectively. When several dipoles are very close to each other, the overlap of their field radiation patterns leads to a dipolar photonic event. Such cooperative coupling creates the macroscopic radiation modes that are spatially and temporally coherent and appear as specular reflection. This fact was recently demonstrated by us for the oscillating photochromic dipoles embedded in a polymeric matrix.[25,26] This phenomenon is applicable to any resonating Hertzian point dipole (bound and free electrons). To confirm this fact, we investigated the specular reflection and the Brewster effect of a nanocomposite composed of Ag nanoparticles (4–5 nm in diameter) embedded in a transparent silica (SiO_2) matrix (20% filling factor) (Figure S1, Supporting Information) via a standard ellipsometry measurement. The details of fabrication, characterization, and calculation of the effective properties of the nanocomposite have been described elsewhere.[27]

Figure 2a–e shows the total and polarized specular reflection properties of a 20 nm film of the nanocomposite under oblique incidence. The light excites the charges to oscillate with the same frequency and to radiate secondary waves.[24,25] The superposition of the secondary waves creates an elastically radiated field that appears as a specular reflection peak at 442 nm (Figure 2a). It is obvious that the peak at 442 nm is smeared when the incidence angle rises from 45° to 75°, and a new peak emerges at 345 nm. To illustrate the phenomenon, the polarized reflection (under s- and p-polarized light illumination) is considered. In the case of the s-polarized light reflection (Rs), the specular reflection peak

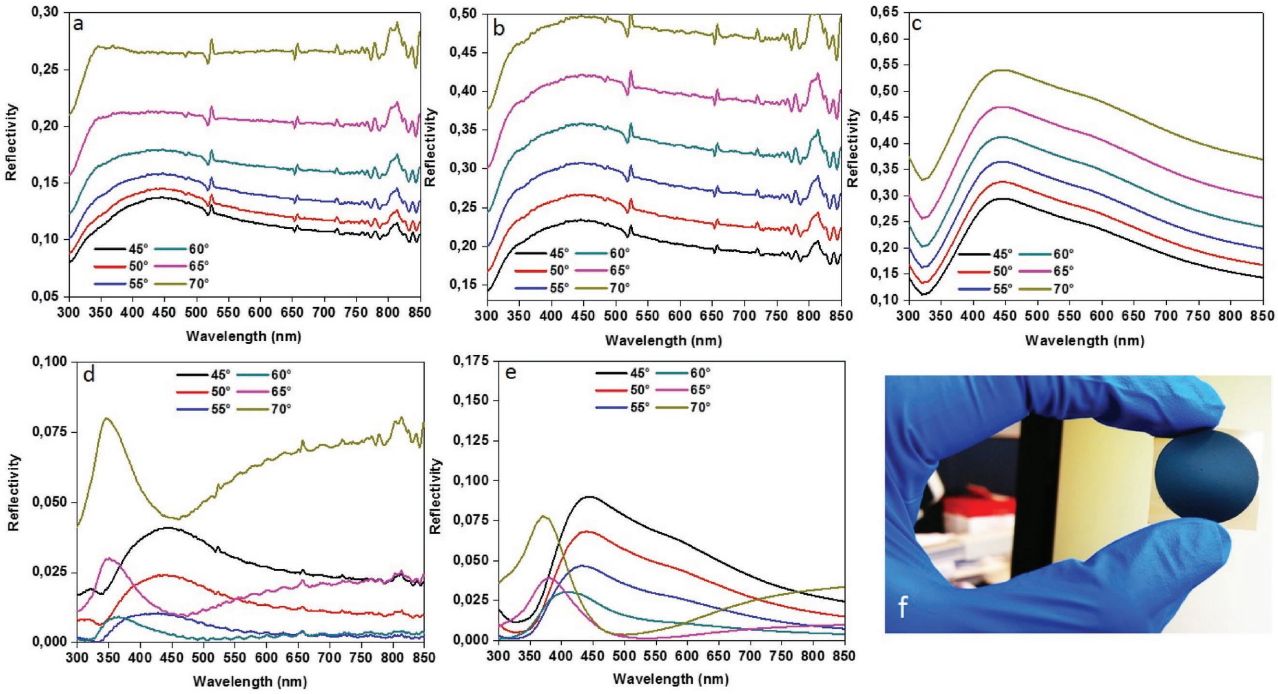

Figure 2. Specular reflection by a plasmonic nanocomposite. a) The total specular reflection spectra of a 20 nm Ag/SiO_2 nanocomposite in various oblique incidence angles. The experimental b) and simulation c) based s-polarized specular reflection spectra of the 20 nm Ag/SiO_2 nanocomposite in various oblique incidence angles. The experimental d) and simulation e) based p-polarized specular reflection spectra of the 20 nm Ag/SiO_2 nanocomposite in various oblique incidence angles. f) Camera image of a carbon tape coated with a thin layer of the nanocomposite.

appears at 442 nm (Figure 2b,c). Since the oscillation direction of electric dipoles is always parallel to that of the reflected light, Rs increased gradually with increasing the incidence angle. A totally different trend was observed for p-polarized light (Figure 2d,e), and the gradually vanishing reflection of the peak at 442 nm was accompanied by a reflection dip at the angle of 65°. It is well known that magnetic induction, i.e., the radiated field polarized within the plane of incidence, can be observed under illumination with p-polarized light. It is characterized by diminishing the radiation once the incident light becomes perpendicular to the axis of the oscillating dipole antenna. As a result, the cooperative dipolar Brewster phenomenon emerges.[24,25]

The simulation data of the polarized specular reflection properties of the 20 nm thin film under oblique incidence for the stratified media (Figure 2c,e) are in good agreement with the corresponding experimental data (Figure 2b,d). The simulation data were calculated via a thin-film transfer matrix approach (to measure the simulated reflection vs wavelength) and by assigning effective optical properties of the nanocomposite.[27]

According to the specular reflection response shown in Figure 2a, the Ag-based plasmonic nanocomposite should appear blue,[28] yet not observable by naked eyes. To visualize the blue color, a black substrate is used, whereby light transmission and diffuse scattering are blocked and the color originates exclusively from the specular plasmonic radiation event. The visualization of the macroscopic blue (reflection based) and yellow (absorption based) colors for the nanocomposites deposited on a black carbon tape and then on a transparent flexible polymer is demonstrated in Figure 2f. Although it is common to deposit or embed plasmonic dipoles in a transparent (neutral) matrix, a blackbody host or substrate is a new alternative for neutral hosting that has not been examined. Here, the dipolar reflection and the Brewster phenomenon are tailored by the well-known plasmonic parameters including size, filling factor, type of the resonating dipole, and medium polarity. **Figure 3**a demonstrates the adjustment of the plasmonic colors of ≈3, 4, and 5 nm Ag deposited on transparent flexible polymer substrates and carbon tapes. The tunability of the extinction colors (yellow, blue, and red) emerged on the plastic foils was characterized in transmission mode, as presented in Figure 3b. In addition, the specularly reflected colors (dark blue, dark green, and yellowish green) emerged on the black carbon tapes were characterized in reflection mode, as shown in Figure 3c. Figure 3d stresses on this fact that by increasing the Ag thickness from 3 to 5 nm, the corresponding plasmonic peaks and the Brewster wavelength occurring at the Brewster angle of 65° are red shifted. Figure S2 (Supporting Information) demonstrates shape, size distribution, and interparticle spacing of the Ag nanoparticles across the host material.

It is worthy to note that the environmental sensitivity of the plasmonic reflection color with respect to the host (surrounding) matrix is much higher than that of the transmitted/extinct light. Because it relies on the propagation delay, the change of the "real part" of RI occurs. This point is visualized in Figure 3e–g. In Figure 3e, a dense assembly of Ag nanomirrors sputtered at 500 °C is seen that is subsequently covered by dielectrics of SiO_2, AlN, and composites made thereof at different ratios and thicknesses. Due to relying solely on the intensity changes, naked-eye detection of color differences of the coated samples in transmission mode is challenging (Figure 3f). Whereas, as seen in Figure 3g,

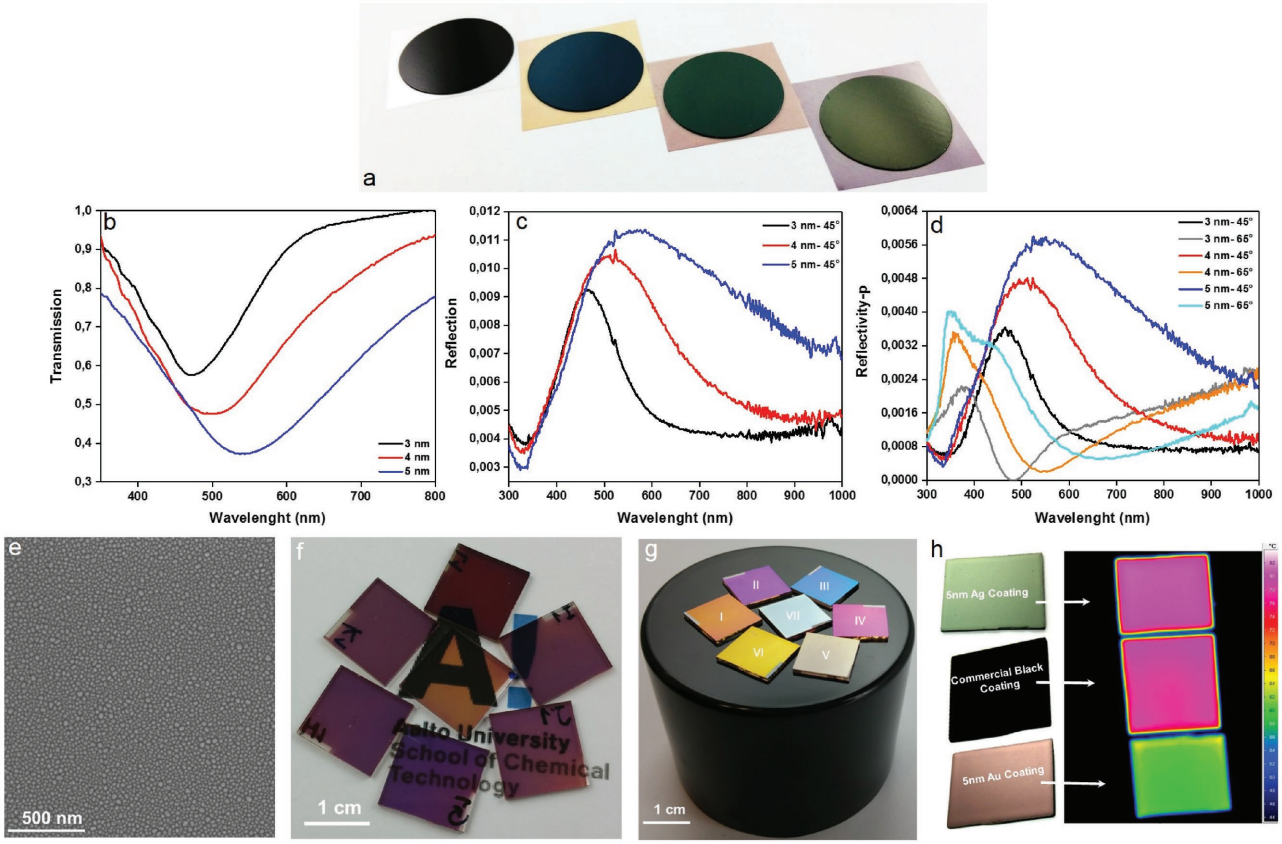

Figure 3. Visualizing the specular reflection color by a blackbody substrate. a) Photograph of the samples comprising 3, 4, and 5 nm thick Ag coatings (left to right) deposited on transparent flexible polymer substrates and carbon tapes (the first sample has no Ag coating). b) Transmission spectra of the same samples shown in (a) but deposited on a transparent polymer film. c) Reflectivity spectra of the same samples shown in (b). d) p-polarized light reflection spectra of 3, 4, and 5 nm thick Ag coatings deposited on a carbon tape and measured at 45° and 65°, illustrating the tunability of the Brewster wavelength at the fixed angle of 65°. e) SEM image of the metasurface shows the Ag nanoparticles (8 nm) sputtered at 500 °C whose interspacing is in the range of their diameter. f) The carriers containing Ag nanoparticles covered with various dielectrics of AlN, SiO_2, and the composites thereof show very weak color contrasts in transmission mode. g) The same samples as in (f) placed on a black background to enhance the reflectivity contrast of various colors at a normal angle of incidence. The samples labeled as I through VII contain various dielectric coatings of AlN, SiO_2, and the composites thereof with different compositions and thicknesses (I: 60 nm (70% AlN/SiO_2), II: 80 nm (50% AlN/SiO_2), III: 80 nm (70% AlN/SiO_2), IV: 80 nm (AlN), V: 80 nm (SiO_2), VI: 60 nm (50% AlN/SiO_2), and VII: no dielectric coating). h) The camera image shows the black spray host with and without the green Ag and golden brown Au coating.

the distinct rainbow colors mimicking natural colors are clearly visible on a black substrate, and each one represents a specific coating material, i.e., an optimum environmental sensitivity.

This unique feature can be seen for other plasmonic dipoles like Au as well. However, to design a broad band perfect-colored absorber without diminishing the high emissivity of the blackbody host in the mid-IR, Ag will be the best choice when considering the optical constants of Au and Ag at the mid-IR wavelength of 5 µm. To explore this point while fully exploiting the striking specular radiation properties of plasmonic dipoles for colored solar absorber, we deposited Ag and Au nanoparticles on a commercial black carbon matrix. The commercial carbon spray (Senotherm) which is known as a commercial IR-emissive product was used for this objective and coated with Ag and Au nanoparticles (a 5 nm thick layer). According to our measurements, this thickness is the critical thickness able to induce the plasmonic response (Figure S3, Supporting Information). While the Ag nanoclusters appear in green color, the Au nanoclusters offer a unique golden brown color. Figure 3h is a camera image of the black spray host with and without the green Ag and golden brown Au coating. Implementation of the metallic nanomirrors would not only serve for the new design of colored solar absorbers but also impact on IR emission of the coating. The IR emissivity of the Ag and Au nanoparticles on the blackbody host was recorded using an IR camera, as illustrated in Figure 3h. While the Ag nanoparticles slightly affect the blackbody's emissivity, the Au nanoparticles act as effective metal nanomirrors that diminish the IR emissivity. This finding can be described by the optical constants (including RI (n) and extinction coefficient (k)) of the bulk metals in the IR range. For Au, $n = 2.19$ and $k = 27.7$. While, for Ag, $n = 1.32$ and $k = 36.2$ @ 5 µm.[29] Ag is well known as a low loss material at optical frequencies and acts as a superior absorber in the mid-IR. This situation is opposite for Au nanoparticles.

Conclusively, this approach brings about a new design rule for a perfect-colored absorber in a rational, simple, and cost-effective manner. Our strategy would govern a new generation of plasmonic-radiated colors useful for a wide variety of applications including colored solar materials and finally would allow

the plasmonic response to walk on its two legs, namely absorptions and reflections, as demonstrated.

By now, our main achievement has been based on the specular reflection of nanoparticles at the localized plasmon resonances. This effect can be employed in the design of perfect-colored absorbers with tailored colors and/or emissivity depending on the type of metals. From now on, we switch our attention to the visualized detection and the plasmonic Brewster phenomenon, which in our belief can revolutionize the biodetection technology. Plasmonics has been successfully implemented to detect a wide variety of biomolecules with sensitivity of even a single molecule based on RI monitoring.[30] However, to date, complicated plasmonic biosensing techniques have not been successful in the bulk RI monitoring-based detection that relies on the volume (incorporation) binding of analytes rather than their surface binding.[31] Thus, bulk detection has not found any practical clinical application. The scientific reason behind such incapability is that the plasmonic coupling results in local near-field enhancement with field decay of only a few nanometers. Thus, microscopic, slight changes by the surrounding molecules or even by an ultrathin molecular film whose thickness does not exceed the decay length can be perfectly detected. On the other hand, the change occurring in the near field is not detectable by a far field observer. Thus, the most important challenge could be related to the detection of bulk analytes (thick films) where the microscopic changes are smeared out by averaging the local field and the system becomes an isotropic medium. In other words, any microscopic dipolar change of the surrounding matrix is not detected by the plasmon, i.e., bulk detection cannot be realized.[21]

Here, we aim to address such a challenge. In our belief, the specular radiating plasmon along with the plasmonic Brewster phenomenon could be the key solutions. The collective oscillation of the dipoles leads to cooperative dipolar coupling and interference that lead to formation of a propagating wave in the surrounding. The dipoles act as microscopic antennas able to store energy while radiating the electromagnetic waves, as schematically shown in **Figure 4**a. The near-field region close to an antenna is dominated by the magnetic field, followed by a transition zone wherein the magnetic and electric fields coexist. Finally, there is a far field zone that is controlled by the electric field. The uniqueness of the antenna is in its operation in the far field whereby information is transferred to an observer via a certain radiated color depending on the propagation delay by the surrounding medium. The color can be strongly altered by charge polarization that affects the propagation of the electromagnetic waves. Owing to the different paths of energy propagation, different interference patterns with distinguishable colors emerge that can be observed by a far field observer. Knowing that the wave speed is equal to the product of frequency and wavelength, if the oscillation frequency of a resonating antenna remains constant, the alteration of speed by the surrounding medium can be represented by a corresponding change in the radiated wavelength. For instance, presence of a bulk material atop the antenna can affect the speed of the wave's propagation, depending on its molecular polarizability. As a result, as seen in Figure 4b, the plasmonic blue color of the nanoparticle does no change notably, while different radiation colors emerge.

In this concept, the "Plasmonic Brewster phenomenon," with the angular and/or wavelength dependency, could play a unique role. When p-polarized light penetrates into the bulk sample to be analyzed, the Plasmonic Brewster Wavelength, PBW, shifts from tens of nanometers to hundreds of nanometers and enables bulk biodetection (**Figure 5**a). A similar effect can be realized while testing several analytes at a fixed angle.

As the scientific principle behind the suggested Brewster sensing concept, the Brewster phenomenon diminishes the reflection of p-polarized light due to the nature of a dipole radiation pattern. Under this circumstance, the abrupt phase changes govern high sensitivity (S) for the biosensor, which can be described by Equation (1):[32,33]

$$S_R = \frac{1}{R(\lambda)} \frac{\partial R(\lambda)}{\partial n}\Big|_{\lambda=\lambda_0} \tag{1}$$

where R is the reflectivity, n is the RI, and λ_0 is the wavelength of the minimum reflectivity in air. As deduced from this equation, the sensitivity, S, is at its maximum when R approaches zero. It is worthy to note that the spectral sensitivity estimated via diminishing of reflection is the basis of the surface plasmon polariton detection scheme (the so-called Kretschmann configuration).

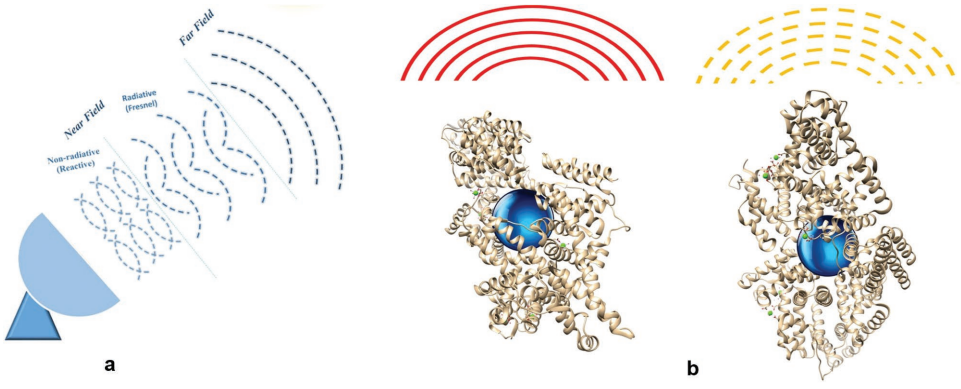

Figure 4. Schematic demonstration of the optical performance of plasmonic dipoles. a) Plasmonic dipoles can be simulated as microscopic antennas able to store energy while radiating the electromagnetic waves. b) Presence of a bovine serum albumin protein containing bulk material atop the antenna can affect the speed of the wave's propagation, so that the plasmonic blue color of the nanoparticle does no change notably, while different radiation colors appear.

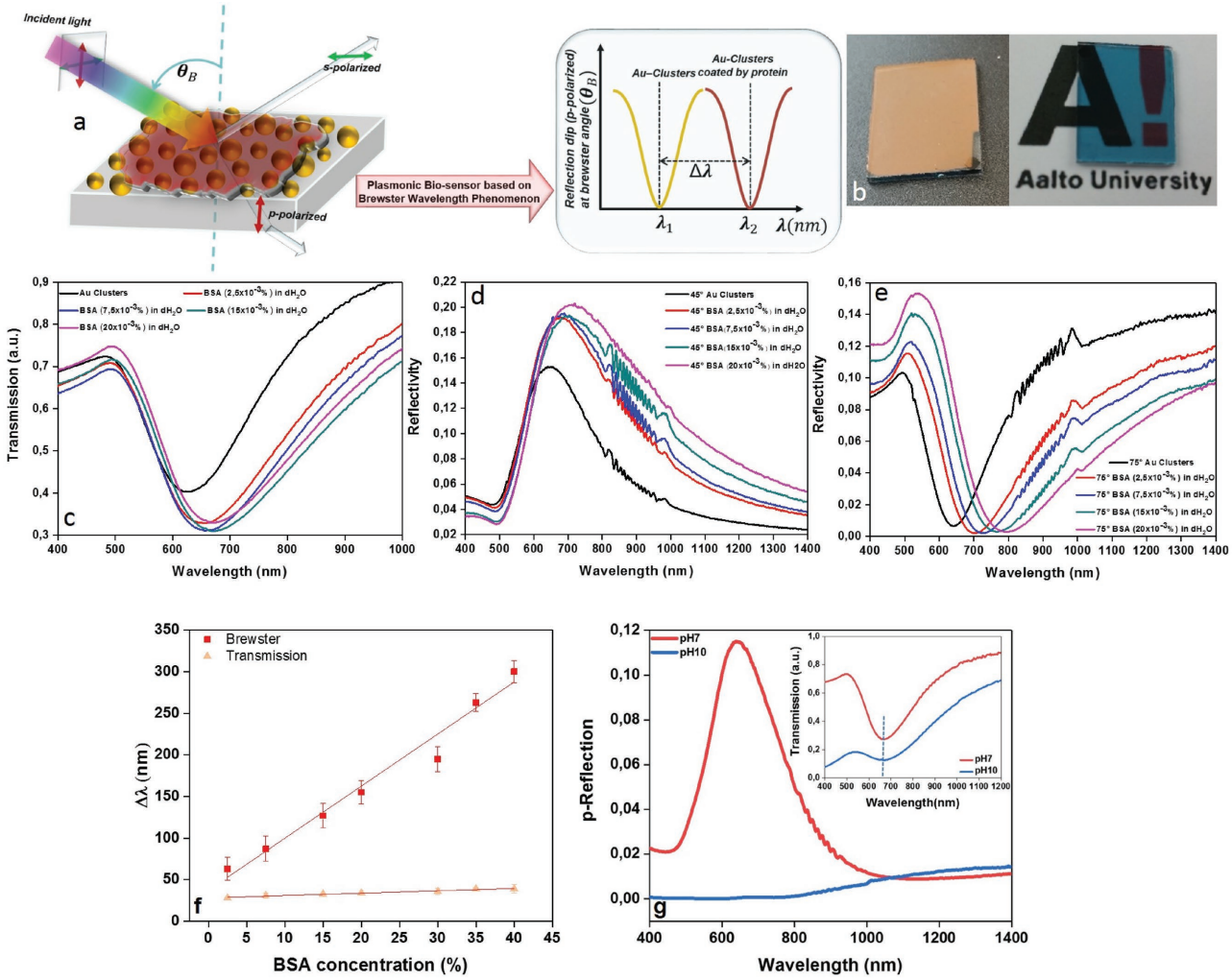

Figure 5. The plasmonic Brewster phenomenon for bulk biosensing. a) Schematic illustration of the phenomenon's mechanism for bulk biosensing where p-polarized light interacts with the analyte and its wavelength shifts. b) Camera images imply different coloration of the deposited nanoclusters in two reflection (left) and transmission (right) modes. c) Transmission spectra of the Au film compared to those of the BSA/Au films (containing different BSA concentrations) implying no significant wavelength shifts, i.e., detectability. d,e) p-polarized light reflection spectra of the Au film and Au/BSA films (containing different BSA concentrations) at an angle below and equal to the Brewster angle, respectively, implying a clear shift of the light's wavelength. The maximum shift occurs at the Brewster angle. f) Linear fit for wavelength shifts ($\Delta\lambda$s) versus BSA's concentration in transmission mode and under the plasmonic Brewster effect. In this figure, standard deviations in measurements ($n = 3$) have been shown by the error bars (in transmission mode, the error bars are as large as the symbols). g) p-polarized light reflection spectra of the Au/BSA films at the Brewster angle of 65° at different pHs (the inset figure, specifically the denoting line, implies that no wavelength shift occurs in transmission mode).

In such a scheme, a specific configuration and optical coupling are necessary to excite the plasmonic response and hence to diminish the reflection at the resonance frequency. However, owing to the limited decay length and plasmonic loss, the detection is limited solely to some molecular binding events onto the metal surface, and it is not applicable for naked-eye and bulk biodetection of samples with different molecular polarizabilities.[21]

Here, as a novel finding and even a breakthrough, we demonstrate the feasibility of naked-eye detection of biological analytes based on bulk RI change. In other words, at the PBW, the detection is based on the change of the RIs' real part (low loss) at the polarizing angle rather than the imaginary part (high loss) applied by the conventional localized plasmon methods. On the other hand, molecular polarizability explains the mutual coupling between the excited dipole antenna and the induced dipole of the surrounding matrix.[25] The coupling varies based on the biomolecules (analytes)' concentration and can be detected using the PBW. In this regard, while surface detection is accomplished by using s- or p-polarized light with an incidence angle of, e.g., below the plasmonic Brewster angle, at the PBW, p-polarized light penetrates into the sample and enables volume detection with high sensitivity. Accordingly, using a micrometer thick film and based on the plasmonic Brewster effect, bulk biodetection is realized that is not attainable by localized plasmonic effects in transmission/extinction or scattering modes.

To examine validity and applicability of our postulate, first, simple biomolecules and, then, human biological samples were considered as analytes. In the latter case, the approach was used to differentiate between the serum exosomes isolated from healthy and diseased individuals. Among the various

plasmonic nanoparticles, Au nanoparticles are highly chemically stable; hence, they are the best choice for fabrication of a plasmonic biosensor.[34] The biosensor was made by sputtering of an Au target at 500 °C (the optical characteristics of the deposited Au film are presented in Figure S4a,b, Supporting Information), thereby forming a dense assembly of nanoparticles (Figure S5, Supporting Information). The camera images shown in Figure 5b exhibit the deposited nanoclusters with different colors in reflection and transmission modes. To demonstrate applicability of the PBW technique, its detection ability for different concentrations of simple commercial bovine serum albumin (BSA) was examined. A BSA suspension with different concentrations was drop cast on the Au nanoparticles to form a micrometer thick film. The extinction measurements in transmission mode, Figure 5c, show no meaningful change when the biomolecule's concentration in the dried film alters. In contrary, when p-polarized light is applied at an angle below the Brewster angle, the high concentrations of the biomolecule are detectable (Figure 5d). Such detectability is at its highest level, as represented by a clear and regular wavelength shift, when p-polarized light penetrates and interacts with the bulk sample at the Brewster angle, Figure 5e, validating our concept. The sensing analytical performance of the PBW sensor in the transmission and Brewster modes is shown in Figure 5f, which plots the wavelength shift versus different concentrations of BSA. As shown in this figure, there is an excellent linear fitness (represented by R^2 values approaching 1) between the BSA concentrations and wavelength shifts for the both modes. The slope of the linear fitted lines implies the response sensitivity of the biosensor,[35] which is much larger in the case of the Brewster mode. The limit of detection (LOD) of the biosensor for BSA protein was calculated through Equation (2) as: LOD = $3S/M$, where S is the standard deviation and M is the slope of the linear fitted curve.[36] The Brewster sensitivity enhancement factor (EF) can be calculated based on the ratio of the slopes in the Brewster and transmission modes, respectively. The calculated R^2 values, slope, LOD, and EF values are tabulated in **Table 1**. As shown in this table, the Brewster sensitivity EF of 22.3 and much lower LOD in the Brewster mode emphasize the optimum sensitivity of our technique for bulk biodetection compared to the transmission/extinction methods.

As another important finding, the biodetection can be carried out according to the Brewster's angle concept. In this regard, the biomolecule-coated nanoparticles are considered as individual effective media with a specific RI. The RI varies depending on the conformation and thus molecular polarizability of the protein shell, influenced by pH. Proportional to the effective RI and the polarizability of the medium, the Brewster angle at which p-polarized light is diminished changes. Figure 5g demonstrates the validation of our concept. This figure implies how p-polarized light interacts with the BSA-coated Au nanoparticles at two different pHs of 7 and 10 at the fixed angle of 65°. It is shown that a reflection dip and peak occur for pH 10 and for pH 7, respectively, indicating that the sample exposed to pH 10 has a lower effective RI than the one subjected to pH 7. This behavior is attributed to the protein denaturation at pH 10, thereby the protein shell becomes less compact compared to that at the lower pH. Most interestingly, the plasmonic wavelength in the extinction measurement does not shift, as illustrated in the inset of Figure 5g, in agreement with our schematic shown in Figure 4b.

Table 1. Analytical performance of the biosensor for BSA and exosome sensing.

	R^2	Slope	LOD [%]	Brewster sensitivity EF
BSA (Transmission)	0.961	0.28 ± 0.022	32.14	–
BSA (Brewster)	0.972	6.25 ± 0.431	7.36	22.3
Exosome (Transmission)	0.998	0.028 ± 0.015	214.28	–
Exosome (Brewster)	0.969	14.43 ± 1.04	4.16	412.3

To benefit our "PBW" concept in real clinical biosensing, i.e., our main goal, we investigated its applicability in the detection of impaired human serum exosomes. Exosomes contain and transport important biological molecules, such as proteins, lipids, micro-RNA, and genetic materials. They are assumed to be impaired in a variety of biological processes and human diseases.[37,38] Thus, tracking their changes can help identify different diseases. Particularly, exosomes could act as inflammatory or even cancer indicators because they carry molecular contents of the cells from which they release.[16] Our concept relies on molecular characteristics of the serum exosomes of healthy and diseased individuals including their specific molecular structures[39] and abundance. These characteristics induce different electromagnetic media for the cooperative plasmonic antenna. Furthermore, tailoring the vesicles' concentration in the sample to be analyzed would change mutual polarizability and thus its detectability by our technique. The serum exosomes analyzed in this study were isolated by using an established precipitation method[40,41] (ExoQuick, SBI/BioCat, Heidelberg, Germany) (see Experimental Section for further details). Similar to the BSA's case, the exosome suspensions were drop cast on Au nanoparticles. Our technique enables naked-eye differentiation of exosomes of healthy individuals and patients in reflection mode, as demonstrated by a camera image in **Figure 6**a. This significant detectability is hardly attainable via an extinction/transmission mode or the current transduction plasmonic detection methods of exosomes.[16,42,43] The obtained results imply drastic differences between the exosomes derived from healthy individuals and inflammatory bowel patients in reflection mode. To prove our hypothesis concerning the applicability of the PBW concept in clinical biodetection, the wavelength shift of p-polarized light when contacting the exosomes derived from healthy individuals and those with inflammatory bowel disease was measured. As shown in Figure 6b,c, the wavelength shift ($\Delta\lambda$) in transmission mode is negligible (less than ≈20 nm), while it is as significant as ≈232 nm at the Brewster angle which implies strong sensitivity of the PBW technique to polarity of the medium. The polarizability change and penetration of p-polarized light into the sample being analyzed at the PBW, enable obvious "bulk" detection. The sensing analytical performance of the PBW sensor in the transmission and Brewster modes is shown in Figure 6d. For both modes, there is a remarkable linear fitness (represented by R^2 values approaching 1) between the exosome concentrations and wavelength shifts. However, the slope of the linear fitted lines that represents the response sensitivity of the biosensor is much larger in the case

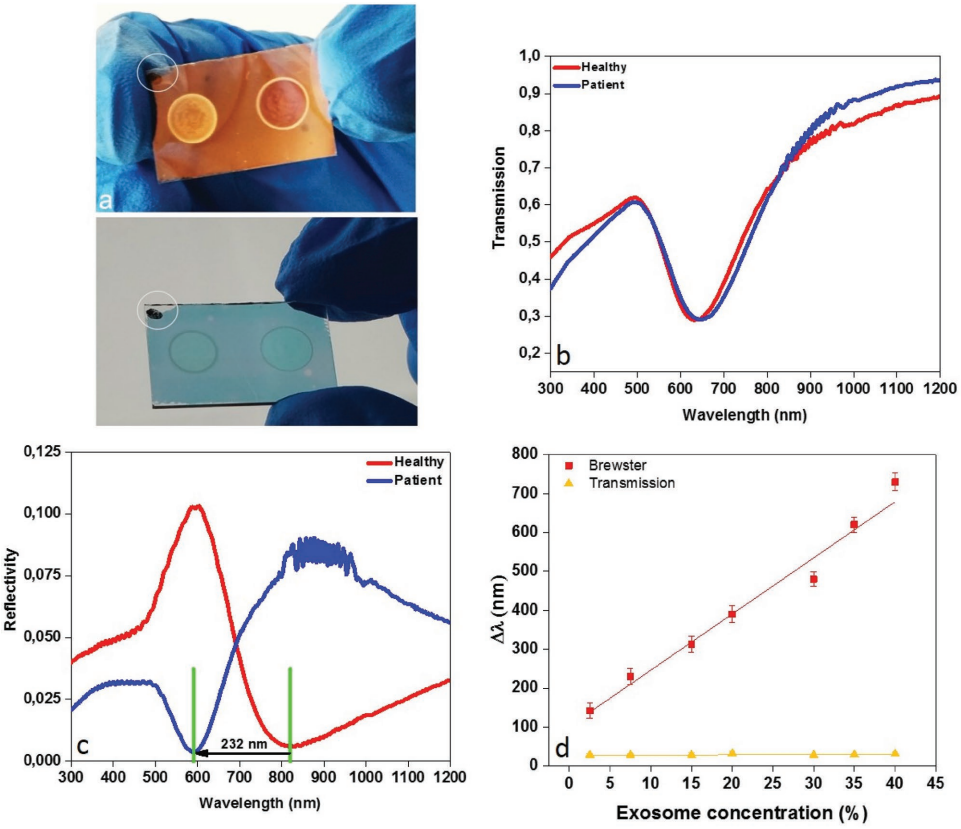

Figure 6. Naked-eye detection of the impaired exosomes via the plasmonic Brewster effect. a) Camera image of the sample containing Au nanoclusters exposed to the serum exosomes isolated from a healthy individual (right) and a patient with inflammatory bowel disease (left) in reflection and transmission modes (top and bottom, respectively) (the circle at the top left corner implies a same biosensing platform but in different optical modes). b) Transmission and c) reflectivity of the Au film coated with the serum exosomes of healthy individuals (red line) and inflammatory bowel patients (blue line). The reflectivity measurement was performed at the 70° angle of incidence, i.e., the Brewster angle. d) Linear fit for wavelength shifts ($\Delta\lambda$s) versus exosome's concentration in transmission mode and under the plasmonic Brewster effect. In this figure, standard deviations in measurements ($n = 3$) have been shown by the error bars (in transmission mode, the error bars are as large as the symbols).

of the Brewster mode. The LOD of the biosensor for exosome was calculated through Equation (2). The Brewster sensitivity EF was measured, as we did for BSA, based on the ratio of the slopes in the Brewster and transmission modes, respectively. The calculated R^2 values, slope, LOD, and EF values for exosome sensing are tabulated in Table 1. Compared to the transmission mode, the Brewster sensitivity EF of 412.3 and much lower LOD in the Brewster mode underline the superior bulk biosensitivity of our technique for exosomes over conventional transmission/extinction methods. While, based on the measured LOD values, our technique is hardly able to compete with surface plasmon polariton (SPP) or localized surface plasmon resonance (LSPR) techniques for molecular sensing, it offers a rapid, convenient recognition method of existence or absence of diseases based on a simple visual inspection.

Taking together, the findings presented here leveraged our comprehension of several optical phenomena based on tiny artificial dipoles. Such outcomes helped identify two amazing optical behaviors of resonating dipolar specular reflection and PBW phenomenon originating from a same plasmonic material. Employing these promising features, a new vision of photonics and structural coloration in the disordered dipolar media on a blackbody and a new platform for hybridized optical and medical devices were realized. With respect to the latter achievement, as we proved, sensitivity of such a novel PBW sensor is far higher than that of the available plasmonic transduction sensors. In addition to bulk biosensing, our approach enables detection of any dielectrics including inorganic coatings.

On the other hand, our technique is indeed simple, cost effective, and scalable, and offers interesting potentials for designing perfect-colored absorbers and visual diagnostic applications. The PBW technique presented here is regarded as a novel, promising approach for a negligibly invasive (blood) clinical analysis.

Experimental Section

The Ag/SiO_2 nanocomposites were fabricated via cosputtering of the metals and SiO_2 on a rotatable substrate. The sputtering chamber was lab made, and all the experiments were conducted under a pressure of 10^{-3} mbar. The sputtering was done with Ar as the inlet gas. Commercial carbon tapes were used as substrates. The filling factor was determined by a quartz glass balance, and thickness of the film was measured based on nominal thickness of the constituting materials. The Ag and Au clusters were made by deposition of Ag and Au at 500 °C followed by cooling down to room temperature inside the vacuum chamber. The Ag sample was coated by 60 nm AlN and

SiO_2 hybrid films. The hybrid coating was prepared by cosputtering of SiO_2 and AlN in the vacuum chamber. The Au samples were used for biosensing measurements as follows.

The detection measurements were done by dropping a 30 µL water-diluted vesicle suspension and BSA solution on the high-temperature deposited Au sample. BSA (dried powder) was purchased from Sigma-Aldrich Co. (USA). It was dissolved in distilled water (5 mg mL^{-1}) and then diluted to make solutions with given concentrations of 2.5, 7.5, 15, and 20×10^{-3}%. The blood serum-derived vesicles were isolated by precipitation using ExoQuick reagent (SBI/BioCat, Heidelberg, Germany) according to the manufacturer's recommendations. Briefly, blood was collected from clinical patients prior to a cancer surgery from a central venous line and from healthy volunteers by aspiration from the medial cubital vein. All the donors gave informed consent to the study, which was approved by the local ethics board. The reference number of the ethics approval was A110/99, issued by the local review board of the Medical Faculty of the Christian-Albrechts-University Kiel. The blood samples were collected in serum-monovettes (Sarstedt, Nürmbrecht, Germany) and were centrifuged at room temperature for 10 min at $2000 \times g$ after blood clotting for the preparation of serum. The sera were stored at −80 °C until a further use. The vesicle fraction was prepared from 500 µL serum samples of each individual. Each serum sample was mixed with a 126 µL ExoQuick reagent, incubated for 30 min at 4 °C for particle precipitation, and subsequently centrifuged at $1500 \times g$ for 30 min at 4 °C.

Optical characterizations of the samples were done by spectroscopic ellipsometry (M-2000 ellipsometer from J.A. Woollam Co., Inc. (Lincoln, America)). By employing a continuously rotating compensator near the sample and a CCD spectrometer, this system enabled concurrent spectral read-out from 190 to 1700 nm. This system measured both transmitted and reflected optical properties over a wide range of incident angles. Data acquisition was performed using the company's CompleteEASE software. The instrument provided reflection, transmission as well as polarization response data of the films and clusters.

Supporting Information

Supporting Information is available from the Wiley Online Library or from the author.

Acknowledgements

M.E. thanks the School of Chemical Engineering at the Aalto University, Finland, the Helmholtz Association (the Initiative and Networking Fund, No. VH-NG-523), and Helmholtz-Zentrum Geesthacht, Germany, for providing financial support to his research group. The authors gratefully acknowledge partial financial supports from the Academy of Finland and the German Research Foundation (DFG) through SFB677 (C01). The blood samples were supplied by the Kiel CCC-biomaterial-bank, funded by the BMBF (PopGen 2.0 Network/P2N-01EY1103). The authors also thank Carsten Rockstuhl and Valeriya Azovskaya for their precious contributions as simulation (and numerical analysis) and drawing of the schematic of Figure 1a, respectively. A.E. acknowledges a grant from the Cluster of Excellence "Inflammation at Interfaces" of Schleswig-Holstein, Kiel, Germany. Also, M.K.H. would like to acknowledge funding from the European Union's Horizon 2020 research and innovation program under the Marie Sklodowska-Curie grant agreement No. 701597.

Note: The presentation of the author name Moheb Abdelaziz was corrected on January 25, 2018, after initial publication online.

Conflict of Interest

The authors declare no conflict of interest.

Keywords

Brewster effect, clinical biosensors, perfect absorbers, plasmonic dipoles, specular reflection

Received: August 7, 2017
Revised: September 27, 2017
Published online: December 7, 2017

[1] S. Kinoshita, S. Yoshioka, J. Miyazaki, *Rep. Prog. Phys.* **2008**, *71*, 076401.
[2] U. Kreibig, M. Vollmer, *Optical Properties of Metal Clusters*, Springer, Heidelberg **1995**.
[3] G. Mie, *Ann. phys.* **1908**, *330*, 377.
[4] V. S. K. Chakravadhanula, M. Elbahri, U. Schùrmann, H. Takele, H. Greve, V. Zaporojtchenko, F. Faupel, *Nanotechnology* **2008**, *19*, 22.
[5] M. K. Hedayati, S. Fahr, C. Etrich, F. Faupel, C. Rockstuhl, M. Elbahri, *Nanoscale* **2014**, *6*, 6037.
[6] C. M. Watts, X. Liu, W. J. Padilla, *Adv. Mater.* **2012**, *24*, OP98.
[7] H. A. Atwater, A. Polman, *Nat. Mater.* **2010**, *9*, 205.
[8] M. K. Hedayati, M. Javaherirahim, B. Mozooni, R. Abdelaziz, A. Tavassolizadeh, V. S. K. Chakravadhanula, V. Zaporojtchenko, T. Strunkus, F. Faupel, M. Elbahri, *Adv. Mater.* **2011**, *23*, 5410.
[9] I. E. Khodasevych, L. Wang, A. Mitchell, G. Rosengarten, *Adv. Opt. Mater.* **2015**, *3*, 852.
[10] K. Kumar, H. Duan, R. S. Hegde, S. C. W. Koh, J. N. Wei, J. K. W. Yang, *Nat. Nanotechnol.* **2012**, *7*, 557.
[11] J. S. Clausen, E. Højlund-Nielsen, A. B. Christiansen, S. Yazdi, M. Grajower, H. Taha, U. Levy, A. Kristensen, N. A. Mortensen, *Nano Lett.* **2014**, *14*, 4499.
[12] J. Olson, A. Manjavacas, L. Liu, W. S. Chang, B. Foerster, N. S. King, M. W. Knight, P. Nordlander, N. J. Halas, S. Link, *Proc. Natl. Acad. Sci.* **2014**, *111*, 14348.
[13] X. Zhu, C. Vannahme, E. Højlund-Nielsen, N. A. Mortensen, A. Kristensen, *Nat. Nanotechnol.* **2015**, *11*, 325.
[14] A. Kristensen, J. K. W. Yang, S. I. Bozhevolnyi, S. Link, P. Nordlander, N. J. Halas, N. A. Mortensen, *Nat. Rev. Mater.* **2016**, *2*, 16088.
[15] G. L. Liu, Y. Yin, S. Kunchakarra, B. Mukherjee, D. Gerion, S. D. Jett, D. G. Bear, J. W. Gray, A. P. Alivisatos, L. P. Lee, F. F. Chen, *Nat. Nanotechnol.* **2006**, *1*, 47.
[16] H. Im, H. Shao, Y. Park, V. Peterson, C. Castro, R. Weissleder, H. Lee, *Nat. Biotechnol.* **2014**, *32*, 490.
[17] V. Kravets, F. Schedin, R. Jalil, L. Britnell, R. Gorbachev, D. Ansell, B. Thackray, K. S. Novoselov, A. K. Geim, A. V. Kabashin, A. N. Grigorenko, *Nat. Mater.* **2013**, *12*, 304.
[18] J. N. Anker, W. P. Hall, O. Lyandres, N. C. Shah, J. Zhao, R. P. Van Duyne, *Nat. Mater.* **2008**, *7*, 442.
[19] C. Sönnichsen, B. M. Reinhard, J. Liphardt, A. P. Alivisatos, *Nat. Biotechnol.* **2005**, *23*, 741.
[20] M. Li, S. K. Cushing, N. Wu, *Analyst* **2015**, *140*, 386.
[21] A. R. Halpern, Y. Chen, R. M. Corn, D. Kim, *Anal. Chem.* **2011**, *83*, 2801.
[22] H. G. Schantz, *IEEE Antennas Propag. Mag.* **2001**, *43*, 50.
[23] A. Doicu, T. Wriedt, Y. A. Eremin, *Light Scattering by Systems of Particles: Null-field Method with Discrete Sources: Theory and Programs*, Springer, Heidelberg **2006**.
[24] J. D. Jackson, *Classical Electrodynamics*, Wiley, New York **1975**.
[25] M. Elbahri, A. U. Zillohu, B. Gothe, M. K. Hedayati, R. Abdelaziz, H. J. El-Khozondar, M. Bawa'aneh, M. Abdelaziz, A. Lavrinenko, S. Zhukovski, S. Homaeigohar, *Light: Sci. Appl.* **2015**, *4*, e316.

[26] M. K. Hedayati, M. Javaheri, A. U. Zillohu, H. J. El-Khozondar, M. S. Bawa'aneh, A. Lavrinenko, F. Faupel, M. Elbahri, *Adv. Opt. Mater.* **2014**, *2*, 705.
[27] C. Etrich, S. Fahr, M. K. Hedayati, F. Faupel, M. Elbahri, C. Rockstuhl, *Materials* **2014**, *7*, 727.
[28] J. A. Izatt, E. A. Swanson, J. G. Fujimoto, M. R. Hee, G. M. Owen, *Opt. Lett.* **1994**, *19*, 590.
[29] M. A. Ordal, L. L. Long, R. J. Bell, S. E. Bell, R. R. Bell, R. W. Alexander Jr., C. A. Ward, *Appl. Opt.* **1983**, *22*, 1099.
[30] J. Masson, *ACS Sensors* **2017**, *2*, 16.
[31] M. C. Estevez, M. A. Otte, B. Sepulveda, L. M. Lechuga, *Anal. Chim. Acta* **2014**, *806*, 55.
[32] N. Liu, M. Mesch, T. Weiss, M. Hentschel, H. Giessen, *Nano Lett.* **2010**, *10*, 2342.
[33] J. Becker, A. Trugler, A. Jakab, U. Hohenester, C. Sönnichsen, *Plasmonics* **2010**, *5*, 161.
[34] S. Zeng, K. T. Yong, I. Roy, X. Q. Dinh, X. Yu, F. Luan, *Plasmonics* **2011**, *6*, 491.
[35] K. V. Sreekanth, Y. Alapan, M. ElKabbash, E. Ilker, M. Hinczewski, U. A. Gurkan, A. De Luca, G. Strangi, *Nat. Mater.* **2016**, *15*, 621.
[36] J. Wu, Y. Chen, M. Yang, Y. Wang, C. Zhang, M. Yang, J. Sun, M. Xie, X. Jiang, *Anal. Chim. Acta* **2017**, *982*, 138.
[37] C. Corrado, S. Raimondo, A. Chiesi, F. Ciccia, G. De Leo, R. Alessandro, *Int. J. Mol. Sci.* **2013**, *14*, 5338.
[38] D. Sun, X. Zhuang, S. Zhang, Z. Deng, W. Grizzle, D. Miller, H. Zhang, *Adv. Drug Delivery Rev.* **2013**, *65*, 342.
[39] H. G. Zhang, W. E. Grizzle, *Am. J. Pathol.* **2014**, *184*, 28.
[40] K. Rekker, M. Saare, A. Roost, A. Kubo, N. Zarovni, A. Chiesi, A. Salumets, M. Peters, *Clin. Biochem.* **2014**, *47*, 135.
[41] H. W. King, M. Z. Michael, J. M. Gleadle, *BMC Cancer* **2012**, *12*, 1.
[42] J. Rak, *J. Front. Pharmacol.* **2013**, *4*, 21.
[43] S. A. Melo, L. B. Luecke, C. Kahlert, A. F. Fernandez, S. T. Gammon, J. Kaye, V. S. LeBleu, E. A. Mittendorf, J. Weitz, N. Rahbari, C. Reissfelder, C. Pilarsky, M. F. Fraga, D. Piwnica-Worms, R. Kalluri, *Nature* **2015**, *523*, 177.